THE JOURNAL OF PHYSICAL CHEMISTRY A

Article

pubs.acs.org/JPCA

Pulse Propagation Effects in Optical 2D Fourier-Transform Spectroscopy: Experiment

Hebin Li,[†] Austin P. Spencer,[‡] Andrew Kortyna,[†,§] Galan Moody,[†,∥] David M. Jonas,[‡] and Steven T. Cundiff*[,†,∥]

[†]JILA, University of Colorado and National Institute of Standards and Technology, Boulder, Colorado 80309-0440, United States

[‡]Department of Chemistry and Biochemistry, University of Colorado, Boulder, Colorado 80309-0215, United States

[§]Department of Physics, Lafayette College, Easton, Pennsylvania 18042, United States

[∥]Department of Physics, University of Colorado, Boulder, Colorado 80309-0440, United States

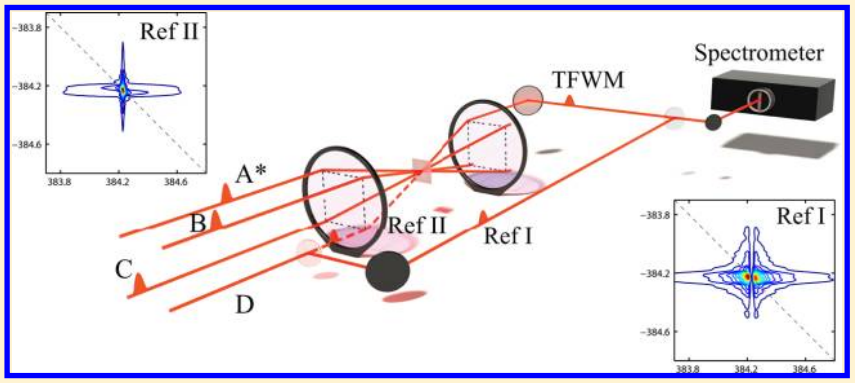

ABSTRACT: In optical two-dimensional Fourier-transform (2DFT) spectroscopy, understanding how the spectral line shape is affected by pulse propagation in the sample is crucial for an accurate interpretation of spectra. We report an experimental study of pulse propagation effects in 2DFT spectroscopy performed in a dense atomic vapor. The spectral line shape can be dramatically distorted due to high optical density as well as the physical thickness of a sample. The spectral distortion can be partially corrected by using a reference pulse copropagating with the signal combined with appropriate data processing.

1. INTRODUCTION

Optical two-dimensional Fourier-transform (2DFT) spectroscopy has been developed into a powerful tool for studying the coupling and dynamics in complex processes such as structural dynamics in proteins,[1] the transient nature of hydrogen bonds in water,[2] energy transfer in photosynthesis,[3,4] and many-body interactions in semiconductor quantum wells,[5,6] semiconductor quantum dots,[7,8] and atomic vapors.[9] 2DFT spectra can reveal unique structural and dynamical information that is not accessible by other techniques, and much of the information is extracted not only from peak positions and strengths but also from line shapes. For example, 2DFT spectroscopy can clearly separate homogeneous broadening from inhomogeneous broadening. Inhomogeneity in a sample can be easily identified from the elongation of spectral peaks in the diagonal direction, and quantitative information about homogeneous and inhomogeneous line widths can be acquired by analyzing the line shapes.[10,11] However, 2DFT spectra might have spectral artifacts due to experimental complications. For instance, Thompson and Wright[12] have studied the spectral artifacts from absorption and refractive index dispersion at infrared resonances. 2DFT spectral line shapes can also be significantly distorted in optically thick samples where pulse propagation can reshape both the excitation pulses and the signal[13,14] unless the reflection geometry[15] is used. Accurate interpretation of 2D spectra taken in transmission geometry must account for pulse propagation effects if the sample is dispersive or optically dense.

Understanding the effects of pulse propagation in 2DFT spectroscopy is important for extending the applications of 2DFT spectroscopy to new samples and processes that require high optical density. Identification and elimination of pulse propagation effects will reveal the desired physical processes in optically dense media, such as many-body interactions, non-Markovian dynamics, and local field effects. It should also enable accurate investigation of the microscopic nonlinear response in optically thick samples. In practice, increasing the optical thickness has the practical advantage of improving signal strengths and signal-to-noise ratios. The flexibility of sample selection will make the sample preparation easier and extend the scope of samples that can be studied.

When a laser pulse propagates through a resonant medium, both its temporal and frequency profile can be modified. For

Special Issue: Prof. John C. Wright Festschrift

Received: January 23, 2013
Revised: March 29, 2013
Published: April 6, 2013

   dx.doi.org/10.1021/jp4007872 | J. Phys. Chem. A 2013, 117, 6279−6287

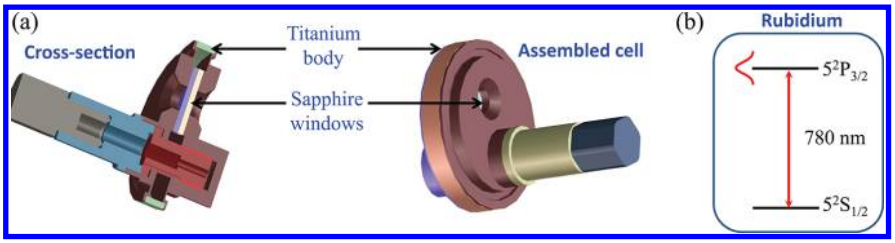

Figure 1. (a) Design of titanium cell that holds rubidium vapor. (b) Relevant energy levels of the rubidium atom.

example, the light absorbed in various parts of the sample can be reradiated. This reradiation interferes with the original field and with the reradiation from previously traveled parts of the sample, resulting in a reshaped field. In the time domain, this process appears as a delay of the original pulse and as a tail or oscillation on the original pulse.[16,17] In a nonlinear experiment with multiple pulses, both excitation pulses and signal field can be altered as they propagate through the sample. Furthermore, the time ordering of the excitation pulses can be scrambled due to temporal profile distortions.[18] It has been shown that the time ordering of the pulse sequence has significant effects on four-wave mixing processes.[19,20] Therefore, various parts of the sample experience different excitation fields and the resulting signals experience different propagation paths. This can profoundly affect the results of experiments. Pulse propagation effects have been studied, both theoretically and experimentally, in photon echo experiments[21−23] and transient four-wave mixing (TFWM) experiments in dense atomic vapors,[24,25] semiconductors,[26] and general optically dense systems.[27]

As an extension of multiple-pulse nonlinear experiments, 2DFT spectroscopy also suffers from spectral artifacts due to pulse propagation effects.[28] Theoretical models have been developed to include propagation effects in calculating 2DFT spectra. Keusters and Warren[29] used a perturbative method[30,31] in which the field acting on any one slice of the sample is the superposition of the original field entering the sample and the re-emitted fields from all earlier slices. This model is only valid for relatively low optical density because only the first-order term in the perturbative expansion of the reshaped field is considered. For high optical density, the pulse distortion can be strong enough to scramble the time ordering of pulses. They later developed a model[32] based on the self-consistent Maxwell−Bloch equations that can be numerically solved to include all propagation effects in the sample. A more sophisticated method, based on the solution of Maxwell's equations in the three-dimensional frequency domain,[33] can treat the propagation effects in media with arbitrary optical density as well as other distortions due to phase matching and detection geometry.[13]

Despite the extensive theoretical investigations of propagation effects in 2DFT spectroscopy, to the best of our knowledge, no experimental work has been done to validate theoretical models beyond tests in the incoherent (large waiting time T) limit. Here we report a systematic experimental study of propagation effects in 2DFT spectroscopy. The experiments are performed in a dense atomic vapor whose optical density can be continuously varied over 1 order of magnitude. The obtained spectra provide insight into the spectral distortion caused by pulse propagation effects due to high optical density as well as the physical thickness of the sample. Besides understanding how pulse propagation affects 2DFT spectra, it is important to seek experimental techniques to correct or reduce spectral distortions. Our results also suggest the possibility of using a copropagating reference pulse and appropriate data processing to reduce the spectral distortion in 2DFT spectra. Moreover, our experiment demonstrates an ideal platform for studying pulse propagation effects in 2DFT spectroscopy.

2. EXPERIMENTAL SECTION

2.1. Sample. The sample is a rubidium atomic vapor loaded into a vapor cell. Figure 1a displays an assembled cell and its cross section. The cell body is made of titanium. Optical access is provided by two sapphire windows that are diffusion bonded to the titanium body.[34] The windows are slightly wedged and have an antireflection coating on the outside surfaces. The gap between the two windows holds a thin layer of atomic vapor as the sample for experiment. The sample thickness for these experiments is about 500 μm.

The cell is loaded with a small amount of rubidium metal with natural isotopic abundance and a 1500 Torr argon buffer gas. The atomic density of rubidium vapor is determined by the temperature of the molten rubidium metal in the cell through the equation of state.[35] It is assumed that the presence of the laser beams does not alter the atomic density. In the experiment, the cell temperature is controlled by a heater to adjust the atomic density (2.14×10^{12} to approximately 1.28×10^{14} cm^{-3} in the current experiment), so that the optical density of the sample can be continuously varied.

The laser spectrum is centered at 780 nm, which is the wavelength of the D_2 line of a rubidium atom. The nearby D_1 line at 795 nm is not excited due to the limited bandwidth of the laser. The D_2-line transition is pressure broadened by the argon buffer gas such that the hyperfine sublevels are neither resolvable nor relevant to the current experiment. Therefore, the system can be considered as a simple two-level system, as shown in Figure 1b.

An alkali metal atomic vapor is an ideal model system for the study of pulse propagation effects in 2DFT spectroscopy. The optical density of the sample can be continuously varied within a large range by simply changing the cell temperature. The system dynamics are relatively simple and have been well characterized using 2DFT spectroscopy and fit to a homogeneous Bloch model,[36] so propagation effects can be isolated from other complications that occur in more complex systems such as molecules or semiconductors. Moreover, unlike a semiconductor, the optical response of an atomic vapor is not sensitive to the pre-excitation by a weak reference pulse so that two different detection geometries, as described in the following section, can be used.

2.2. Experiment. Our implementation of 2DFT spectroscopy is based on TFWM experiments performed in the box geometry. The output from a mode-locked Ti:sapphire laser is split into four identical, phase-stabilized pulses within the JILA-

dx.doi.org/10.1021/jp4007872 | J. Phys. Chem. A 2013, 117, 6279−6287

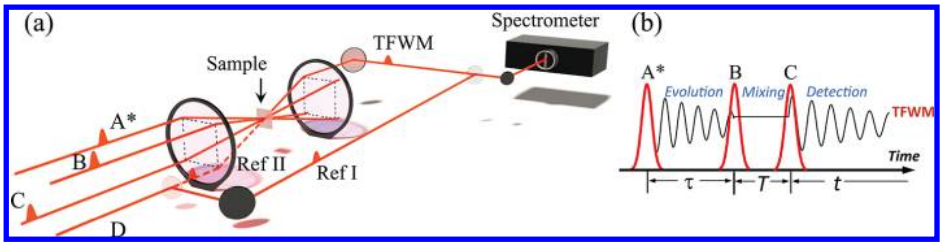

Figure 2. (a) Schematic diagram of 2DFT spectroscopic apparatus. (b) Time ordering of the excitation pulses.

MONSTR,[37] which is an interferometer of two Michelson interferometers with active phase-stabilization. As shown in Figure 2a, four pulses propagate along the corners of a square with sides of 1 in. Three pulses (A*, B, and C) are focused on the sample by a 15 cm lens to generate a TFWM signal that propagates along the fourth corner of the square. The beam diameter at the half-maximum intensity is 50 μm, and the Rayleigh range is about 1 cm. The time delay of each pulse can be controlled independently. The time ordering of the pulses are shown in Figure 2b. There are three time periods: τ between the first and second pulses, T between the second and third pulses, and the radiation time t. The resulting signal is denoted as the rephasing signal, $S_I(\tau,T,t)$, if the conjugated pulse A* arrives first, and as the nonrephasing signal, $S_{II}(\tau,T,t)$, if the conjugated pulse A* arrives second. Only the rephasing pulse ordering is used in the present study, although propagation effects can bring in contributions from other pulse orderings. The TFWM signal is spectrally resolved and heterodyne detected with a local oscillator (the reference pulse, D) using spectral interferometry. A 2DFT spectrum $S_I(\omega_\tau,T,\omega_t)$ is constructed by Fourier-transforming the signal with respect to time period τ while the radiation axis is measured in the frequency domain by the spectrometer.

There are two detection geometries in 2DFT experiments with heterodyne detection. In the first case, the reference beam is routed around the sample, as shown by the path labeled "ref I", and is later combined with the signal on a beam splitter. This is referred to as "reference around the sample". In the second case, the reference beam passes through the sample, as shown by the path (dash line) labeled "ref II", and copropagates with the signal. This is referred to as "reference through the sample". With a chosen detection geometry, the reference beam path that is not used is blocked during the experiments. In the first geometry, the reference pulse does not excite the sample prior to or after the excitation pulses. This fact is important for the samples whose nonlinear optical response is sensitive to the pre-excitation of the sample, such as semiconductors. The reference pulse does not experience propagation effects beyond a time delay and mirror phase shifts because it does not go through the sample. In the second geometry, however, the reference pulse experiences absorptive, dispersive, and focal propagation effects in the sample. Because the reference pulse experiences phase distortions similar to those of the signal, the distorted reference pulse can act to cancel the spectral phase distortion in 2DFT spectra. However, the absorptive distortions of reference and signal pulse amplitude do not cancel. Both detection geometries are implemented to investigate pulse propagation effects in 2DFT spectroscopy and how effectively the spectral phase distortion can be corrected by passing the reference through the sample.

2.3. Data Analysis. For each step of the time delay τ, the TFWM signal field is retrieved from spectral interferometry[38] between the TFWM signal and the reference. The TFWM signal $\hat{E}_S$ and the reference pulse $\hat{E}_R$ are

$$\hat{E}_S = \tilde{E}_S(\omega)e^{-i\omega\tau_S}e^{i\phi_S(\omega)} \quad (1)$$

$$\hat{E}_R = \tilde{E}_R(\omega)e^{-i\omega\tau_R}e^{i\phi_R(\omega)} \quad (2)$$

where $\tilde{E}_{S,R}$, $\tau_{S,R}$, and $\phi_{S,R}$ are the real-valued reduced electric field, the delay, and the spectral phase, respectively. The spectral phase contains all pulse chirp if the pulses are not transform-limited. In the experiment, the intensity of the interferogram of the TFWM signal and the reference is recorded by the spectrometer,

$$I_{SI} = |\hat{E}_S + \hat{E}_R|^2 = |\hat{E}_S|^2 + |\hat{E}_R|^2 + \hat{E}_S\hat{E}_R^* + \hat{E}_S^*\hat{E}_R \quad (3)$$

The spectra of the TFWM signal and reference are also recorded individually and are given by $I_{TFWM} = |\hat{E}_S|^2$ and $I_{ref} = |\hat{E}_R|^2$, respectively. The spectra of the TFWM signal and reference are subtracted from the interferogram ($I_{SI} - I_{TFWM} - I_{ref}$), leaving only the interference terms of which the term $\hat{E}_S\hat{E}_R^*$ is chosen via Fourier filtering for the following processing. Alternatively, the terms $|\hat{E}_S|^2$ and $|\hat{E}_R|^2$ can be eliminated through phase cycling.[37,39−41] The interference term of interest is

$$\hat{E}_S\hat{E}_R^* = \tilde{E}_S\tilde{E}_R e^{i\phi_S(\omega)}e^{-i\phi_R(\omega)}e^{-i\omega(\tau_S-\tau_R)} \quad (4)$$

This interference term is numerically Fourier-transformed into the time domain to retrieve a time-resolved TFWM signal. Because the TFWM signal is only expected after pulse C in the absence of propagation distortions, the time-domain signal is filtered by setting the amplitude to zero before pulse C arrives to reduce the noise due to scatter from excitation pulses. The filtered signal is then Fourier-transformed back into the frequency domain. The interference term is divided by the amplitude (with or without the phase term) of the reference field giving

$$\frac{\hat{E}_S\hat{E}_R^*}{|\tilde{E}_R|} = \tilde{E}_S e^{i\phi_S(\omega)}e^{-i\phi_R(\omega)}e^{-i\omega(\tau_S-\tau_R)} \quad (5a)$$

$$\frac{\hat{E}_S\hat{E}_R^*}{\tilde{E}_R e^{-i\phi_R(\omega)}} = \tilde{E}_S e^{i\phi_S(\omega)}e^{-i\omega(\tau_S-\tau_R)} \quad (5b)$$

These equations give the amplitude of the TFWM signal. To obtain the phase of the TFWM signal relative to the excitation fields, the time delay $\tau_S-\tau_R$ can be measured and the phase ϕ_R relative to the reference input can be determined by differential pump−probe[42] or all-optical[43] methods. In the case where the reference is routed around the sample, the reference phase ϕ_R is a constant across the pulse spectrum and eq 5a can be used. In the case where the reference goes through the sample, the reference pulse is also distorted due to the propagation. As a

dx.doi.org/10.1021/jp4007872 | J. Phys. Chem. A 2013, 117, 6279−6287

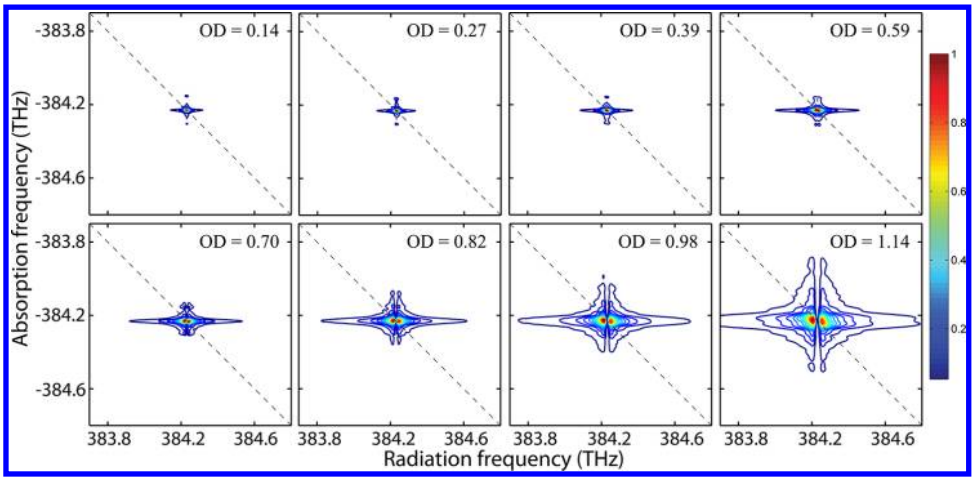

Figure 3. Experimental 2DFT amplitude spectra of rubidium D_2 line at different optical densities. The spectra are taken with the reference beam routed around the sample.

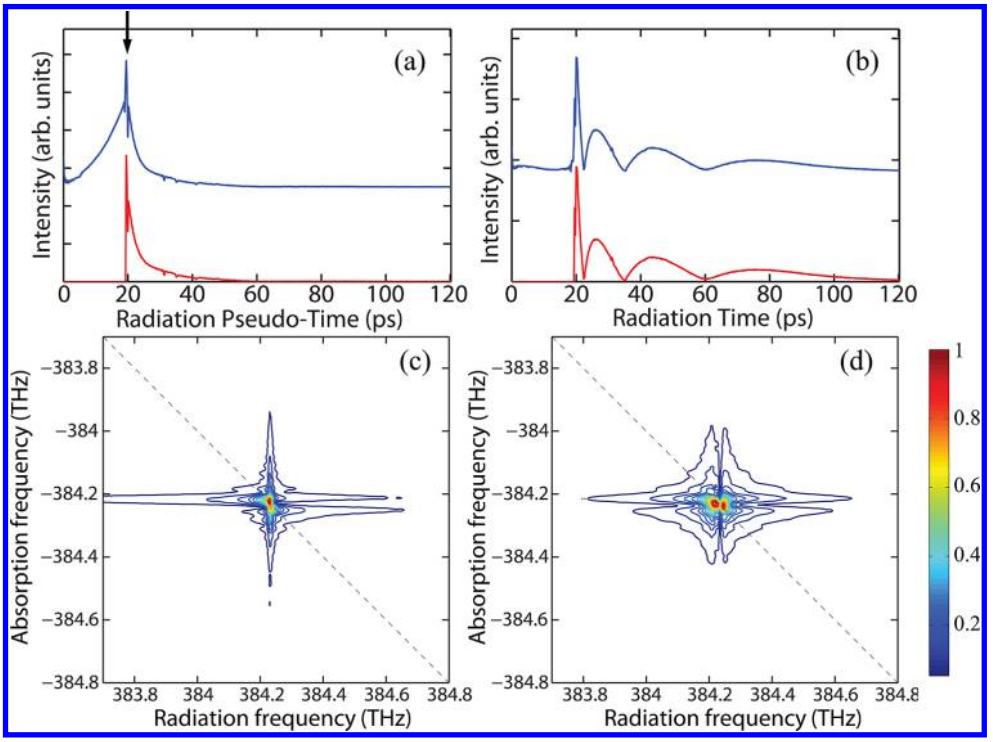

Figure 4. Absolute value of the temporal envelope of the time-resolved TFWM signal retrieved from interferograms without (a) and with (b) inclusion of the phase of the reference pulse. Blue curves are the original signal (offset for clarity), and red curves are the truncated signal used for generating 2DFT spectra. The corresponding 2DFT spectra are generated without (c) and with (d) inclusion of the phase of the reference pulse. The spectra are measured at OD = 0.67.

result, the phase of the reference $\phi_R(\omega)$ is no longer a constant, but a function of frequency. The reference spectral phase needs to be measured and eq 5b can be used to retrieve the TFWM signal. The same process is repeated to retrieve the TFWM spectrum for each step of time delay τ. A 2DFT spectrum is generated by Fourier transforming a series of TFWM spectra with respect to time delay τ.

3. RESULTS AND DISCUSSION

Only rephasing 2DFT spectra are taken in the current experiment. The waiting time T is set to 200 fs for all measurements. The laser repetition rate is 76 MHz, the pulse duration (the intensity full width half-maximum) is about 150 fs, the average power of each excitation beam is 10 mW and the excitation beams are collinearly polarized. 2DFT spectra are obtained with two detection geometries. In one case, the reference beam is routed around the sample. In the other, the reference beam goes through the sample. The data that are reported in this article were taken with the laser repetition rate at 76 MHz. We have also taken data with the laser repetition rate at 250 kHz. The data show quantitative differences but no qualitative differences between the two repetition rates.

3.1. Optical Density (OD) Dependence. 2DFT experiments are performed with a rubidium vapor at different optical densities. As discussed above, the optical density (OD) of the vapor is controlled by the cell temperature. The actual OD at a

dx.doi.org/10.1021/jp4007872 | J. Phys. Chem. A 2013, 117, 6279−6287

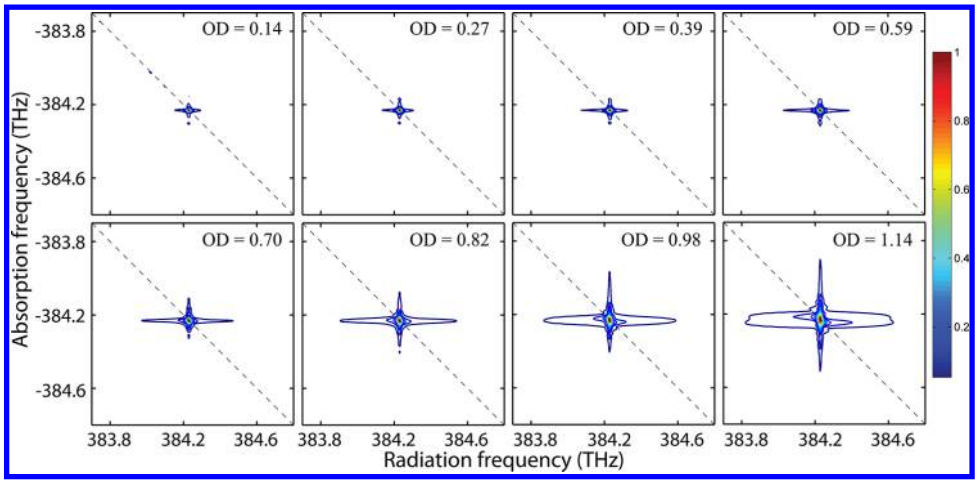

Figure 5. Experimental 2DFT amplitude spectra of rubidium D_2 line at different optical densities. The spectra are taken with the reference beam going through the sample.

given temperature is experimentally determined through a linear absorption measurement. In this article, the OD is defined as OD = $-\log_{10}(T)$, where T is the transmission at the center frequency of the resonance.

3.1.1. Reference around the Sample. In the case where the reference beam is routed around the sample, the reference pulse does not experience absorptive and dispersive propagation effects. The resulting 2D spectra reflect the propagation effects on the excitation pulses and TFWM signal. Figure 3 shows the 2D amplitude spectra obtained at different OD's ranging from 0.14 to 1.14. The horizontal axes are the radiation frequency, and the vertical axes are the absorption frequency, which is plotted as negative for rephasing spectra. The dotted diagonal line indicates equal and opposite absorption and radiation frequencies. The spectra are plotted with 20 evenly spaced contours, and the maximum value of each spectrum is normalized to one.

At very low OD (0.14), the 2DFT amplitude spectrum is a standard star-shaped peak on the diagonal line, which is expected for a homogeneous two-level system.[11] The 2D star is asymmetrically broadened along the radiation frequency direction. This asymmetry is not understood, as the absolute value rephasing 2D spectra for a Bloch model have the symmetrical 2D star peak shape. As the temperature and OD increase, the spectrum becomes broader, more asymmetric, and distorted. The faster dephasing rate due to elevated temperatures is partially responsible for the spectral broadening; however, it should not cause any asymmetry in the spectra. It has been shown[29] that the propagation effect is not symmetric along the absorption and radiation frequency directions, and the spectral distortion along the radiation frequency direction is more severe than along the absorption frequency direction. In Figure 3, the spectrum is broadened more along the radiation frequency direction as the OD increases. The spectrum eventually starts splitting at OD = 0.59, and a gap is clearly formed in the spectrum at OD = 1.14. Such a splitting in 2DFT spectra was not predicted by previous theoretical models at these optical densities.[13,29,32]

Qualitatively, a spectral distortion along the radiation frequency axis arises from resonant reabsorption of the TFWM signal. Through depletion near the line center, reabsorption results in a broader line shape in the radiation frequency direction at modest OD. At high OD, the signal at the resonant frequency can be completely absorbed, resulting in a spectral gap. The spectrum can also be severely distorted in the absorption frequency direction if the excitation pulses experience strong propagation effects prior to generating the TFWM signal. This effect will be discussed in section 3.2.

3.1.2. Reference through the Sample. In the case where the reference goes through the sample, the reference pulse also experiences propagation effects. Particularly, the phase of the reference pulse is distorted so that the phase $\phi_R(\omega)$ is a function of frequency. Without correcting the reference phase, the time-resolved signal retrieved from an interferogram through eq 5a is not on a true time axis; we call it pseudo-time.[44] Figure 4a shows a retrieved time-resolved TFWM signal as the blue curve, which is vertically offset for clarity. The arrow marks the time when the maximum intensity part of pulse C arrives at the sample exit. The signal appears both before and after pulse C due to the distorted phase of the reference. To correct the phase, the phase distortion of the reference pulse, $\phi_R(\omega)$, can be characterized through spectral interferometry between paths "ref I" and "ref II", where "ref II" acts as a local oscillator. Specifically, the interferogram and the spectra of both "ref I" and "ref II" are recorded. The interference term can be obtained by subtracting the spectra of "ref I" and "ref II" from the interferogram. The phase of the reference "ref I" can be extracted from the interference term. Using eq 5b, the measured $\phi_R(\omega)$ cancels out the phase term $e^{-i\phi_R(\omega)}$ in eq 5a, and the retrieved signal as a function of true time is shown in Figure 4b as the blue curve, which is also vertically offset. With the reference phase corrected, the signal appears after pulse C and shows oscillations due to the propagation effects distorting the signal.

To process the data for generating a 2DFT spectrum, the interferograms at all steps of τ are phase corrected by the reference phase. The resulting TFWM signal is not affected by the distortion of the reference pulse, and it only includes the propagation effects of excitation pulses and signal. As shown in Figure 4b, the time-resolved signal is truncated such that the signal after the peak of pulse C (red curve) is taken for constructing a 2DFT spectrum. The generated 2DFT amplitude spectrum is shown in Figure 4d. The spectrum is distorted along both the absorption and radiation frequency directions, indicating that both the excitation pulses and the TFWM signal experience propagation effects. When the phase

dx.doi.org/10.1021/jp4007872 | J. Phys. Chem. A 2013, 117, 6279−6287

and amplitude of the reference pulse at the sample exit are included, the spectra measured with this detection geometry should be equivalent to the ones measured with the detection geometry with the reference going around the sample, if other experimental conditions are the same. In both cases, the spectra are distorted by propagation effects of the excitation pulses and the TFWM signal.

An alternative processing algorithm keeps the reference's phase distortion in the spectral interferogram. Because the reference pulse copropagates with the signal, they experience the same propagation distortions in the sample. Therefore, the phase distortion in the reference pulse can correct the phase distortion in the signal. In fact, this correction automatically takes place in interferograms processed using eq 5a in which the signal phase ϕ_S and the reference phase ϕ_R have opposite signs. Figure 4a shows the time-resolved signal (blue curve) without correcting the phase. The signal after pulse C (red curve) is used to construct a 2DFT spectrum. The generated 2DFT amplitude spectrum is shown in Figure 4c. The spectrum is distorted along the absorption frequency direction, but the higher contours of the line shape do not show severe distortion along the radiation frequency direction compared to a star-shaped 2DFT spectrum (such as observed at low OD). This suggests that the distortion in the reference pulse, when combined with pseudo-time-domain truncation before pulse C, is able to remove some distortions of the 2DFT amplitude peak shape.

To demonstrate the effectiveness of using a copropagating reference pulse to reduce signal propagation effects, 2DFT spectra at different OD's are acquired under the same experimental conditions as the 2DFT spectra in Figure 3, with the only difference being that the reference beam goes through the sample for detection. The data processing using eq 5a does not remove the reference's phase distortion. The retrieved time-resolved signal is truncated in pseudo-time to keep only the signal that appears after pulse C. The generated 2DFT amplitude spectra are shown in Figure 5. Compared to Figure 3, the spectrum is less severely distorted along the radiation frequency direction as the OD increases. However, obvious distortions along the absorption frequency direction start to appear at OD = 0.98. Compared to the spectra in Figure 3, the results show that spectral distortions along the radiation frequency direction, which are caused by propagation effects of pulse C and the TFWM signal, can be effectively corrected by the phase of the copropagating reference pulse and appropriate truncation in pseudo-time. In contrast, spectral distortions along the absorption frequency direction, which are due to propagation effects of the excitation pulses, cannot be corrected by the reference pulse. From the spectra, one can tell whether the distortion occurs mainly in the excitation or emission paths. Figure 5 also shows tilt in the spectra. It should be noted that a qualitatively similar tilt was reported in calculations of absorptive/dispersive propagation distortions for the real (absorptive) 2D correlation spectrum of a Bloch model dominated by lifetime dephasing (see Figure 5a,b of ref 13). The exact cause of the tilt requires further investigation.

3.2. Effects of Sample's Physical Thickness. Besides optical density, the physical thickness of a sample also plays a crucial role in affecting the line shape of 2DFT spectra, especially when the sample thickness is greater than the overlap length of the excitation beams. In the box geometry, generation of a TFWM signal occurs only in the region where all excitation beams spatially overlap. The size of the region is determined by the beam size and the crossing angle between beams. In our experiment, using the beam diameter at the half-intensity, the beam overlap (L, as shown in Figure 6) is estimated to be 400

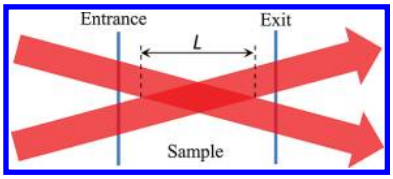

Figure 6. Position of beam overlap relative to the entrance or exit of sample. Only two beams are shown for simplicity.

μm along optical axis, whereas the sample thickness is about 500 μm. As shown in Figure 6, the position of sample with respect to the beam overlap is important. If the beam overlap is closer to the entrance, the excitation pulses are not appreciably affected by propagation whereas the TFWM signal is. If the beam overlap is closer to the exit, the excitation pulses experience more propagation effects and the TFWM signal less.

The exact position of the sample relative to the beam overlap can dramatically modify the line shape of 2DFT spectra. To demonstrate this effect, 2DFT spectra are acquired with different sample positions while the OD remains constant (OD = 0.84). The obtained spectra are shown in Figure 7. The values above the spectra represent relative sample positions at which the spectra are taken. A lower value indicates that the beam overlap is closer to the entrance, whereas a higher value means that the beam overlap is closer to the exit. The positions are not the distance between the beam overlap and the entrance or exit. The sample position at which the TFWM signal has maximum amplitude is chosen as zero. This position might be slightly different in the two data sets presented below.

The 2DFT spectra in the upper row are acquired with the reference beam routed around the sample. At the position (−200 μm) where the beam overlap is closest to the entrance, the spectrum is severely distorted only along the radiation frequency direction, featuring a spectral gap. As the beam overlap moves closer to the exit, the spectrum becomes more distorted along the absorption frequency direction. At the position (300 μm) closest to the exit, the spectrum is severely distorted along both directions. This distortion arises from the excitation pulses being reshaped by the propagation before TFWM takes place. To better visualize the distortion in both directions and its dependence on the sample position, the 2DFT spectra are projected onto the radiation frequency axis and the absorption frequency axis. Parts a and b of Figure 8 show the representative projections onto the radiation frequency axis and the absorption frequency axis, respectively. The maximum amplitude of the projections are normalized to one. Both (a) and (b) are the projections of the 2DFT spectrum at 0 μm position acquired with the reference around the sample. The distortion generates a valley in both projections. The deeper the valley, the worse the distortion. For the projection (a) onto the radiation frequency axis, the distortion can be characterized by the amplitude of the valley (marked with the red arrow) and the width of the valley (the horizontal distance between the two peaks marked with the blue arrows). The black dots in the inset in (a) show the amplitude and the red squares show the width of the valley at different positions. Although the amplitude and the width vary slightly at different positions, the projections show a strong distortion at all positions. However, the projection (b) onto the

dx.doi.org/10.1021/jp4007872 | J. Phys. Chem. A 2013, 117, 6279−6287

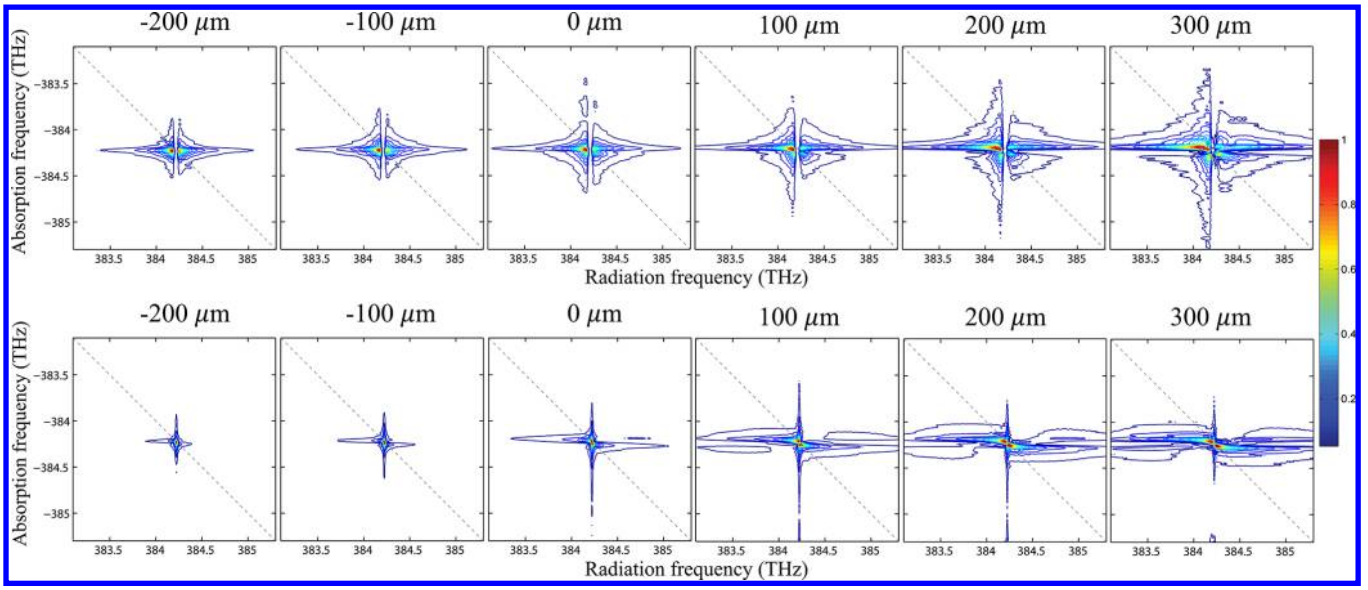

Figure 7. 2DFT amplitude spectra at the different positions of beam overlap. The upper row shows the spectra obtained with the reference routed around the sample. The lower row shows the spectra obtained with the reference going through the sample (these spectra are generated without inclusion of the reference phase in the data analysis).

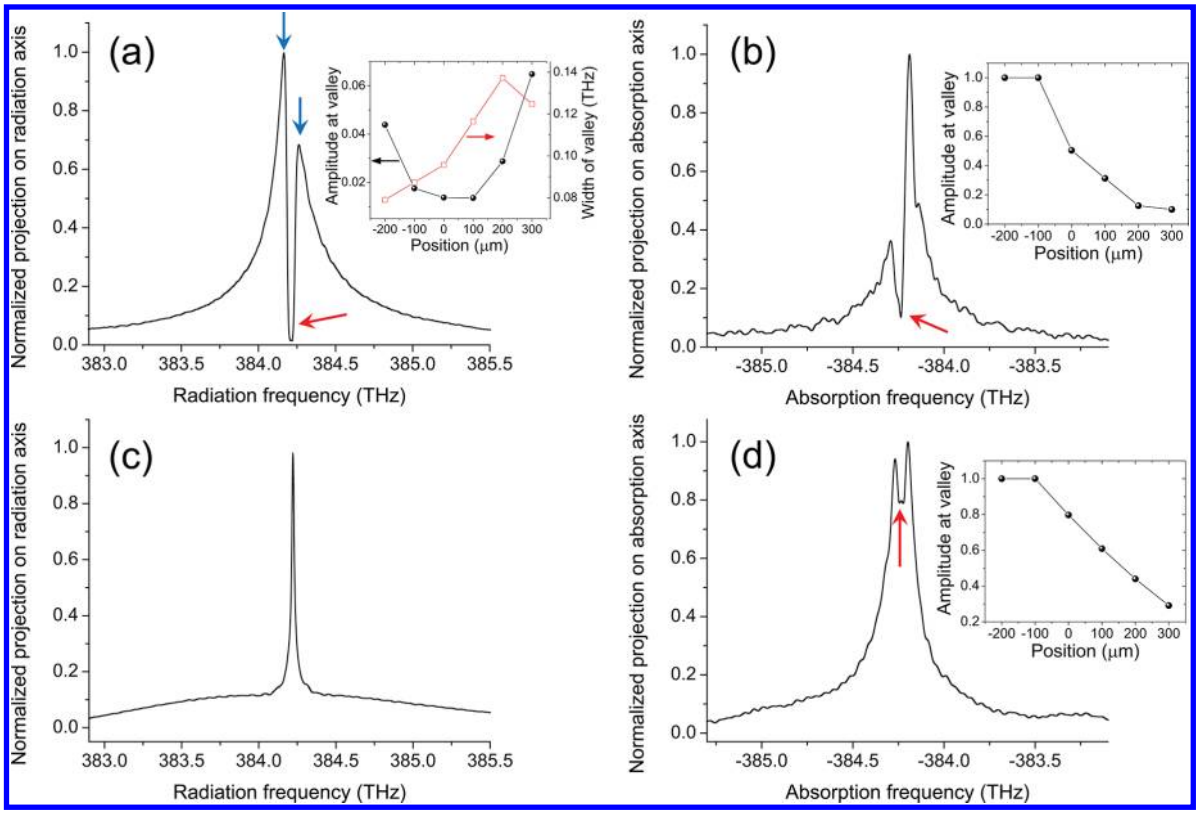

Figure 8. Horizontal and vertical projections of 2DFT spectra. (a) and (b) are the projections in the radiation frequency axis and the absorption frequency axis, respectively, of the 2DFT spectrum at 0 μm position in the upper row in Figure 7. (c) and (d) are the projections in the radiation frequency axis and the absorption frequency axis, respectively, of the 2DFT spectrum at 0 μm position in the lower row in Figure 7. The black dots in the insets show the amplitude at the valley at different sample position. The red squares in the inset in (a) shows the width of the valley at different sample positions.

absorption frequency axis is not always distorted. The amplitude of the valley marked with the red arrow is plotted in the inset. At the positions −200 and −100 μm, the amplitude is one, indicating no distortion. The amplitude decreases as the beam overlap moves closer to the sample exit, indicating more distortion. These results further support that propagation effects in both the excitation pulses and the TFWM signal attribute to the spectral distortion along the radiation frequency direction, whereas spectral distortion along the absorption frequency direction is a manifestation of propagation effects in

dx.doi.org/10.1021/jp4007872 | J. Phys. Chem. A 2013, 117, 6279−6287

the excitation pulses. This is expected from eqs 17 and 18 and the discussion in Appendix A of ref 28.

The lower row in Figure 7 shows the 2DFT spectra acquired with the reference beam routed through the sample. The spectra are generated without inclusion of the phase of the reference pulse. At the position (−200 μm) where the beam overlap is closest to the entrance, the spectrum is not severely broadened even along the radiation frequency direction because the spectral distortion is corrected by the reference pulse. As the beam overlap moves closer to the exit, the spectrum becomes more distorted along the absorption frequency direction, while the spectrum remains less distorted along the radiation frequency direction. Parts c and d of Figure 8 show the representative projections of the 2D spectrum at 0 μm position acquired with the reference through the sample. The projection (c) onto the radiation frequency axis does not have a valley at all sample positions. For the projection (d) onto the absorption frequency axis, the amplitude of the valley marked with the red arrow is plotted in the inset. The projection does not have a valley at the positions −200 and −100 μm, but it is more distorted as the beam overlap moves closer to the sample exit. These results provide further evidence that a copropagating reference pulse can effectively correct propagation effects in the TFWM signal and spectral distortion along the radiation frequency direction but cannot correct propagation effects in the excitation pulses.

4. CONCLUSION

In conclusion, we report a systematic experimental study of pulse propagation effects in 2DFT spectroscopy. The experiments are performed in a dense atomic vapor. We found that 2DFT spectra are broadened at modest OD and split at high OD due to propagation effects. Propagation effects in both the excitation pulses and the TFWM signal show up as spectral distortions along the radiation frequency direction, whereas spectral distortions along the absorption frequency direction are manifestations of propagation effects in the excitation pulses. We also found that the physical thickness of the sample is important. Particularly, the overlap position of beams relative to the sample's entrance or exit changes the propagation effects of TFWM signal and excitation pulses and can dramatically modify the line shape of 2DFT spectra. Two different detection geometries, "reference around the sample" and "reference through the sample", are tested in the experiments. We found that a reference pulse copropagating with the TFWM signal can be used to automatically compensate dispersive propagation effects in the TFWM signal and correct spectral distortion along the radiation frequency direction. However, a copropagating reference pulse is not able to correct propagation effects in the excitation pulses.

Our results provide insights into spectral distortion caused by pulse propagation effects in 2DFT spectroscopy and present experimental evidence to validate theoretical models that help to extract accurate microscopic nonlinear response in optically dense samples. Because of various advantages of atomic vapors, the experiment also demonstrates an ideal experimental platform for studying pulse propagation effects in 2DFT and in higher dimensional[45] spectroscopy.

AUTHOR INFORMATION

Corresponding Author

*E-mail: cundiff@jila.colorado.edu. Phone: +1-303-492-7858. Fax: +1-303-492-5235.

Notes

The authors declare no competing financial interest.

ACKNOWLEDGMENTS

We thank Dr. Bo Sun for discussions and help on the experiment. The work at JILA was primarily supported by the National Science Foundation through the JILA Physics Frontier Center and also by the Chemical Sciences, Geosciences, and Energy Biosciences Division, Office of Basic Energy Science, Office of Science, U.S. Department of Energy under Award #DEFG02-02ER15346. The work of A.P.S. and D.M.J. was supported by National Science Foundation Grant CHE-1112365.

REFERENCES

(1) Hamm, P.; Lim, M.; DeGrado, W. F.; Hochstrasser, R. M. The Two-dimensional IR Nonlinear Spectroscopy of a Cyclic Pentapeptide in Relation to Its Three-dimensional Structure. *Proc. Natl. Acad. Sci. U. S. A.* **1999**, *96*, 2036−2041.

(2) Fecko, C. J.; Eaves, J. D.; Loparo, J. J.; Tokmakoff, A.; Geissler, P. L. Ultrafast Hydrogen-Bond Dynamics in the Infrared Spectroscopy of Water. *Science* **2003**, *301*, 1698−1702.

(3) Brixner, T.; Stenger, J.; Vaswani, H. M.; Cho, M.; Blankenship, R. E.; Fleming, G. R. Two-Dimensional Spectroscopy of Electronic Couplings in Photosynthesis. *Nature* **2005**, *434*, 625−628.

(4) Tiwari, V.; Peters, W. K.; Jonas, D. M. Electronic Resonance with Anticorrelated Pigment Vibrations Drives Photosynthetic Energy Transfer Outside the Adiabatic Framework. *Proc. Natl. Acad. Sci. U. S. A.* **2013**, *110*, 1203−1208.

(5) Li, X.; Zhang, T.; Borca, C. N.; Cundiff, S. T. Many-Body Interactions in Semiconductors Probed by Optical Two-Dimensional Fourier Transform Spectroscopy. *Phys. Rev. Lett.* **2006**, *96*, 057406.

(6) Karaiskaj, D.; Bristow, A. D.; Yang, L.; Dai, X.; Mirin, R. P.; Mukamel, S.; Cundiff, S. T. Two-Quantum Many-Body Coherences in Two-Dimensional Fourier-Transform Spectra of Exciton Resonances in Semiconductor Quantum Wells. *Phys. Rev. Lett.* **2010**, *104*, 117401.

(7) Moody, G.; Singh, R.; Li, H.; Akimov, I.; Bayer, M.; Reuter, D.; Wieck, A.; Bracker, A.; Gammon, D.; Cundiff, S. Influence of Confinement on Biexciton Binding in Semiconductor Quantum Dot Ensembles Measured with Two-dimensional Spectroscopy. *Phys. Rev. B* **2013**, *87*, 041304.

(8) Moody, G.; Singh, R.; Li, H.; Akimov, I. A.; Bayer, M.; Reuter, D.; Wieck, A. D.; Cundiff, S. T. Fifth-Order Nonlinear Optical Response of Excitonic States in an InAs Quantum Dot Ensemble Measured with Two-dimensional Spectroscopy. *Phys. Rev. B* **2013**, *87*, 045313.

(9) Dai, X.; Richter, M.; Li, H.; Bristow, A. D.; Falvo, C.; Mukamel, S.; Cundiff, S. T. Two-Dimensional Double-Quantum Spectra Reveal Collective Resonances in an Atomic Vapor. *Phys. Rev. Lett.* **2012**, *108*, 193201.

(10) Tokmakoff, A. Two-Dimensional Line Shapes Derived from Coherent Third-Order Nonlinear Spectroscopy. *J. Phys. Chem. A* **2000**, *104*, 4247−4255.

(11) Siemens, M. E.; Moody, G.; Li, H.; Bristow, A. D.; Cundiff, S. T. Resonance Lineshapes in Two-Dimensional Fourier Transform Spectroscopy. *Opt. Express* **2010**, *18*, 17699−17708.

(12) Thompson, D. E.; Wright, J. C. Model for Spectral Artifacts in Two-Dimensional Four-Wave Mixing Spectra from Absorption and Refractive Index Dispersion at Infrared Resonances. *J. Phys. Chem. A* **2000**, *104*, 11282−11289.

(13) Yetzbacher, M. K.; Belabas, N.; Kitney, K. A.; Jonas, D. M. Propagation, Beam Geometry, and Detection Distortions of Peak Shapes in Two-Dimensional Fourier Transform Spectra. *J. Chem. Phys.* **2007**, *126*, 044511.

(14) Cho, B.; Yetzbacher, M. K.; Kitney, K. A.; Smith, E. R.; Jonas, D. M. Propagation and Beam Geometry Effects on Two-Dimensional Fourier Transform Spectra of Multilevel Systems. *J. Phys. Chem. A* **2009**, *113*, 13287−13299.

(15) Li, H.; Moody, G.; Cundiff, S. Reflection Optical Two-Dimensional Fourier-Transform Spectroscopy. *Opt. Express* **2013**, *21*, 1687−1692.
(16) Rothenberg, J. E.; Grischkowsky, D.; Balant, A. C. Observation of the Formation of the 0π Pulse. *Phys. Rev. Lett.* **1984**, *53*, 552−555.
(17) Crisp, M. D. Propagation of Small-Area Pulses of Coherent Light through a Resonant Medium. *Phys. Rev. A* **1970**, *1*, 1604−1611.
(18) Wegener, M.; Chemla, D. S.; Schmitt-Rink, S.; Schäfer, W. Line Shape of Time-resolved Four-Wave Mixing. *Phys. Rev. A* **1990**, *42*, 5675−5683.
(19) Lozovoy, V. V.; Pastirk, I.; Brown, E. J.; Grimberg, B. I.; Dantus, M. The Role of Pulse Sequences in Controlling Ultrafast Intramolecular Dynamics with Four-Wave Mixing. *Int. Rev. Phys. Chem* **2000**, *19*, 531−552.
(20) Lozovoy, V. V.; Pastirk, I.; Comstock, M. G.; Dantus, M. Cascaded Free-Induction Decay Four-Wave Mixing. *Chem. Phys.* **2001**, *266*, 205−212.
(21) Olson, R. W.; Lee, H. W. H.; Patterson, F. G.; Fayer, M. D. Optical Density Effects in Photon Echo Experiments. *J. Chem. Phys.* **1982**, *76*, 31−39.
(22) Saikan, S.; Miyamoto, H.; Tosaki, Y.; Fujiwara, A. Optical-Density Effect in Heterodyne-Detected Accumulated Photon Echo. *Phys. Rev. B* **1987**, *36*, 5074−5077.
(23) Christensson, N.; Dietzek, B.; Pascher, T.; Yartsev, A.; Pullerits, T. Three-Pulse Photon Echo Peak Shift in Optically Dense Samples. *Chem. Phys. Lett.* **2008**, *457*, 106−109.
(24) Kinrot, O.; Prior, Y. Four-Wave Mixing in Optically Dense Media. *Phys. Rev. A* **1994**, *50*, R1999−R2002.
(25) Kinrot, O.; Prior, Y. Nonlinear Interaction of Propagating Short Pulses in Optically Dense Media. *Phys. Rev. A* **1995**, *51*, 4996−5007.
(26) Schulze, A.; Knorr, A.; Koch, S. W. Pulse Propagation and Many-Body Effects in Semiconductor Four-Wave Mixing. *Phys. Rev. B* **1995**, *51*, 10601−10609.
(27) Belabas, N.; Jonas, D. M. Fourier Algorithm for Four-Wave-Mixing Signals from Optically Densesystems with Memory. *Opt. Lett.* **2004**, *29*, 1811−1813.
(28) Hybl, J. D.; Ferro, A. A.; Jonas, D. M. Two-Dimensional Fourier Transform Electronic Spectroscopy. *J. Chem. Phys.* **2001**, *115*, 6606−6622.
(29) Keusters, D.; Warren, W. S. Effect of Pulse Propagation on the Two-Dimensional Photon Echo Spectrum of Multilevel Systems. *J. Chem. Phys.* **2003**, *119*, 4478−4489.
(30) Mukamel, S.; Tortschanoff, A. Multiple Quantum Coherences in Liquid State NMR and Nonlinear Optics: Collective VS Local Origin. *Chem. Phys. Lett.* **2002**, *357*, 327−335.
(31) Tortschanoff, A.; Mukamel, S. Collective Many-Body Resonances in Condensed Phase Nonlinear Spectroscopy. *J. Chem. Phys.* **2002**, *116*, 5007−5022.
(32) Keusters, D.; Warren, W. S. Propagation Effects on the Peak Profile in Two-dimensional Optical Photon Echo Spectroscopy. *Chem. Phys. Lett.* **2004**, *383*, 21−24.
(33) Belabas, N.; Jonas, D. M. Three-Dimensional View of Signal Propagation in Femtosecond Four-Wave Mixing with Application to the Boxcars Geometry. *J. Opt. Soc. Am. B* **2005**, *22*, 655−674.
(34) Lorenz, V. O.; Dai, X.; Green, H.; Asnicar, T. R.; Cundiff, S. T. High-Density, High-Temperature Alkali Vapor Cell. *Rev. Sci. Instrum.* **2008**, *79*, 123104.
(35) Nesmeyanov, A. N. *Vapor Pressure Curve of Chemical Elements*; Elsevier: New York, 1963.
(36) Dai, X.; Bristow, A. D.; Karaiskaj, D.; Cundiff, S. T. Two-Dimensional Fourier-Transform Spectroscopy of Potassium Vapor. *Phys. Rev. A* **2010**, *82*, 052503.
(37) Bristow, A. D.; Karaiskaj, D.; Dai, X.; Zhang, T.; Carlsson, C.; Hagen, K. R.; Jimenez, R.; Cundiff, S. T. A Versatile Ultrastable Platform for Optical Multidimensional Fourier-Transform Spectroscopy. *Rev. Sci. Instrum.* **2009**, *80*, 073108.
(38) Lepetit, L.; Chériaux, G.; Joffre, M. Linear Techniques of Phase Measurement by Femtosecond Spectral Interferometry for Applications in Spectroscopy. *J. Opt. Soc. Am. B* **1995**, *12*, 2467−2474.
(39) Tekavec, P. F.; Lott, G. A.; Marcus, A. H. Fluorescence-Detected Two-Dimensional Electronic Coherence Spectroscopy by Acousto-optic Phase Modulation. *J. Chem. Phys.* **2007**, *127*, 214307.
(40) Wagner, W.; Li, C.; Semmlow, J.; Warren, W. Rapid Phase-Cycled Two-Dimensional Optical Spectroscopy in Fluorescence and Transmission Mode. *Opt. Express* **2005**, *13*, 3697−3706.
(41) Shim, S.-H.; Strasfeld, D. B.; Ling, Y. L.; Zanni, M. T. Automated 2D IR Spectroscopy Using a Mid-IR Pulse Shaper and Application of this Technology to the Human Islet Amyloid Polypeptide. *Proc. Natl. Acad. Sci. U. S. A.* **2007**, *104*, 14197−14202.
(42) Jonas, D. M. Two-Dimensional Femtosecond Spectroscopy. *Annu. Rev. Phys. Chem.* **2003**, *54*, 425−463.
(43) Bristow, A. D.; Karaiskaj, D.; Dai, X. C.; Cundiff, S. T. All-Optical Retrieval of the Global Phase for Two-Dimensional Fourier-Transform Spectroscopy. *Opt. Express* **2008**, *16*, 18017−18027.
(44) Pseudo-time should not be confused with the quasi-time conjugate to wavelength that arises in intermediate steps of the spectral interferometry processing algorithm. See: Albrecht, A. W.; Hybl, J. D.; Faeder, S. M. G.; Jonas, D. M. Experimental Distinction between Phase Shifts and Time Delays: Implications for Femtosecond Spectroscopy and Coherent Control of Chemical Reactions. *J. Chem. Phys.* **1999**, *111*, 10934−10956.
(45) Li, H.; Bristow, A. D.; Siemens, M. E.; Moody, G.; Cundiff, S. T. Unraveling Quantum Pathways Using Optical 3D Fourier-Transform Spectroscopy. *Nat. Commun.* **2013**, *4*, 1390.